

Supporting Information

Designing Nitrogen-Enriched Echinus-like Carbon Capsules for Highly Efficient Oxygen Reduction Reaction and Lithium Ion Storage

Chuangang Hu,[†] Lixia Wang,[†] Yang Zhao,[†] Minghui Ye,[†] Qing Chen,[†] Zhihai Feng,[‡] and
Liangti Qu^{*,†}

Characterization

The morphology of the samples was determined by TecnaiG2 20ST (T20) high resolution transmission electron microscopy (HR-TEM) at an acceleration voltage of 120 kV. Field-emission scanning electron microscope (FE-SEM) images and EDS data of the samples were taken on JSM-7001F SEM unit. The elemental mappings were carried out on a scanning transmission electron microscope (STEM) unit with high-angle annular dark-field (HAADF) detector (HITACHI S-5500) operating at 30 kV. X-ray diffraction (XRD) patterns were obtained by using a Netherlands 1,710 diffractometer with a Cu K α irradiation source ($\lambda = 1.54 \text{ \AA}$), and a self-calibration process was performed with a SiO₂ internal standard sample prior to target measurement. Raman spectra were recorded using a RM 2000 Microscopic Confocal Raman Spectrometer (Renishaw PLC, England) with an Ar laser at a wavelength of 514.5 nm. X-ray photoelectron spectroscopy (XPS) data were obtained with an ESCALab220i-XL electron spectrometer from VG Scientific using 300W AlK α radiation. The base pressure was about 3×10^{-9} mbar. The binding energies were referenced to the C 1s line at 284.8 eV from adventitious carbon. Nitrogen adsorption-desorption isotherms were measured on Tristar II (Micrometrics) at 575 K. Pore size distribution and specific surface area were obtained through Barrett-Joyner-

Halenda (BJH) and Brunauer-Emmett-Teller (BET) methods from adsorption branch of the isotherm, at a relative pressure range of $P/P_0 = 0.05-0.25$. The composition of samples was also determined by an elemental analyzer (Vario EI) using combustion method.

Electrochemical measurements

Oxygen Reduction Reaction (ORR) Measurements: The electrochemical measurements for ORR were conducted in a three-electrode cell by using a CHI760D electrochemical workstation. A glass carbon RDE loaded with the electrocatalyst was used as the working electrode, a saturated calomel electrode (SCE) as the reference electrode (calibrated and converted to reversible hydrogen electrode (RHE) through this work), and a Pt wire (0.5 mm in diameter) as the counter electrode. The glassy carbon disk was rinsed with double distilled water and dried at room temperature before the catalyst was loaded to the disk. The working electrode was prepared as follows: 2 mg of catalyst was added into 0.8 mL of ethanol and 80 μ L of 5 wt% perfluorosulfonic acid (PFSA), which is dispersed by ultrasonication for approximately 30 min to obtain a homogeneous suspension. Next, 10 μ L of the dispersion was uniformly dropped onto a freshly polished glassy carbon electrode (5.0 mm in diameter) and was dried under ambient conditions. By using the same electrode configuration, commercial Pt/C on glass carbon catalyst with the same amount was also studied for comparison.

The electrochemical experiments were carried out in O₂ saturated 0.1 M KOH electrolyte for ORR. CV curves were recorded by applying a linear potential scan at a sweep rate of 10 mV s⁻¹ between 0.23 and 1.23 V after purging O₂ or N₂ gas for 30 min. The cycling was repeated until the reproducible CV curves were obtained before the measurement curves were recorded. Measurements on RRDE (ca. 0.25 cm² for disk with a diameter and ca. 0.19 cm² for ring) and/or rotating disk electrode (RDE, 5 mm in diameter) were carried out on a CHI 760D potentiostat equipped with MSR electrode rotator (Pine Instrument) at a scan rate of 10 mV s⁻¹. RDE measurements were conducted at different rotating speeds from 500 to 2500 rpm, and RRDE measurements were carried out at 1500 rpm. Long term durability test of N-CC@CNTs and commercial Pt/C was also conducted for 100 h for N-CC@CNTs and Pt/C with O₂ continuous flow in 0.1 M KOH. All electrochemical experiments were performed at 25 \pm 1 $^{\circ}$ C.

The Koutecky-Levich plots were obtained by linear fitting of the reciprocal rotating speed versus reciprocal current density. The electron transfer number (n) involved in a typical ORR process can be calculated from the slopes of Koutecky-Levich equation (1) as follows:

$$B=0.2nFv^{-1/6}C_{O_2}(D_{O_2})^{2/3} \quad (1)$$

Where n is the number of electrons transferred per oxygen molecule, F is the Faraday constant (96485 C mol^{-1}), D_{O_2} is the diffusion coefficient of O_2 in 0.1 M KOH ($1.9 \times 10^{-5} \text{ cm s}^{-1}$), v is the kinetic viscosity, and C_{O_2} is the concentration of O_2 ($1.2 \times 10^{-3} \text{ mol L}^{-1}$). The constant 0.2 is adopted when the rotating speed is in rpm.

The peroxide percentage ($\%HO_2^-$) was calculated based on the following equation (2):

$$\%HO_2^- = 200 \times I_r / (NI_d + I_r) \quad (2)$$

n was determined from RRDE measurements on the basis of the disk current (I_d) and ring current (I_r) via the following equation (3):

$$n = 4NI_d / (NI_d + I_r) \quad (3)$$

Where N is current collection efficiency of the Pt ring, 0.37.

Lithium ion battery (LIB) measurements: Electrochemical performance of LIB was tested by Swagelok-type LIB cells assembled in an argon filled glove box. For the anode preparation, a mixture of active material, carbon black, and polyvinylidene fluoride (PVDF) binder with a weight ratio of 85:10:5 was dispersed in N-methylpyrrolidone (NMP) solution, and the resultant slurry was then uniformly pasted on a Cu foil current collector. The typical electrode was dried at $120 \text{ }^\circ\text{C}$ for 24 h under vacuum before assembled into coin cell in an argon-filled glove box. A Celgard 2400 microporous polypropylene membrane was used as the separator, and Li foil was used as the counter electrode. The nonaqueous electrolyte used was 1 M $LiPF_6$ dissolved in an ethylene carbonate (EC)/dimethyl carbonate (DMC)/diethyl carbonate (DEC) mixture (1:1:1, in wt%). Galvanostatic cycling experiments of the cells were performed on a LAND CT2001A battery test system in the voltage range of 0.01–3.00 V versus Li^+/Li at room temperature.



Fig. S1 (a) The empty rectangular porcelain boat. (b) The melamine power undergoes the solvothermal treatment at 140 °C as typical experiment in the porcelain boat; (c) The above mentioned melamine power after thermally annealing process at 800 °C. After thermally annealing process, noting left but an empty rectangular porcelain boat, indicating the sublimation process was dominant under high temperature.

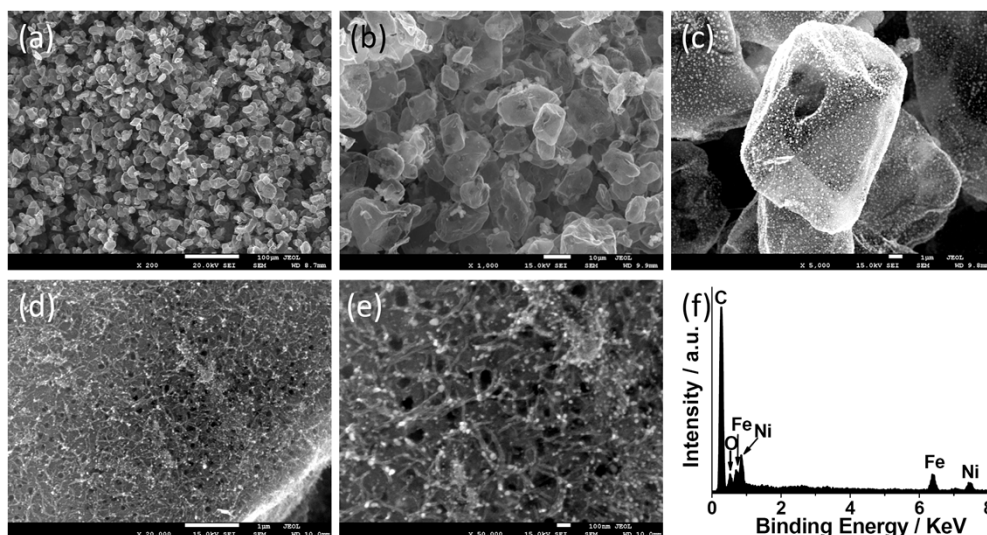


Fig. S2 (a–e) SEM images of N-CC@CNTs before treatment with HCl solution at different magnifications, and (f) the corresponding energy dispersive spectroscopy (EDS). Scale bars: (a), 100 μm ; (b), 10 μm ; (c, d), 1 μm ; (e), 100 nm.

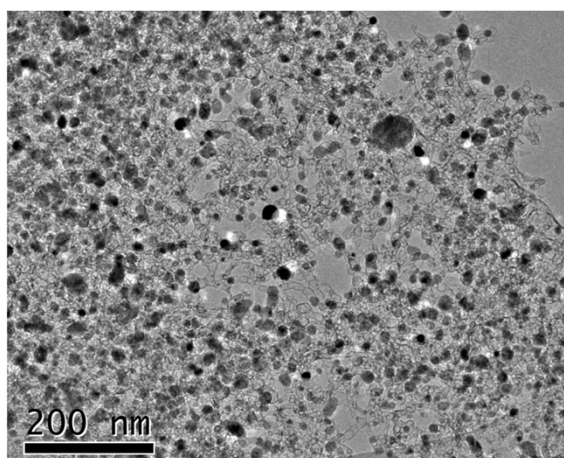


Fig. S3 TEM image of the N-CC@CNTs before treatment with HCl solution.

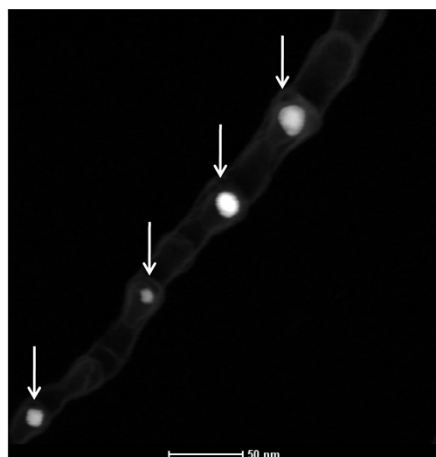


Fig. S4 High-angle annular-dark field scanning transmission electron microscopy (HAADF-STEM) image of the encapsulated FeNi nanoparticles in bamboo-like CNT (as pointed by arrows).

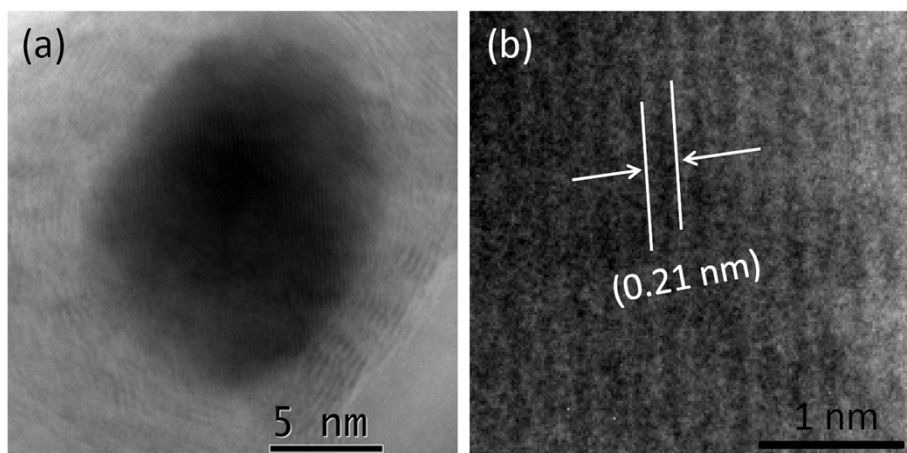


Fig. S5 (a) TEM image of an encapsulated FeNi nanoparticle in CNT. (b) HR-TEM image of the FeNi nanoparticle. The d -space of the crystal plane is 0.21 nm, consistent with the standard d value (0.207 nm) of FeNi alloy (111) plane distance.

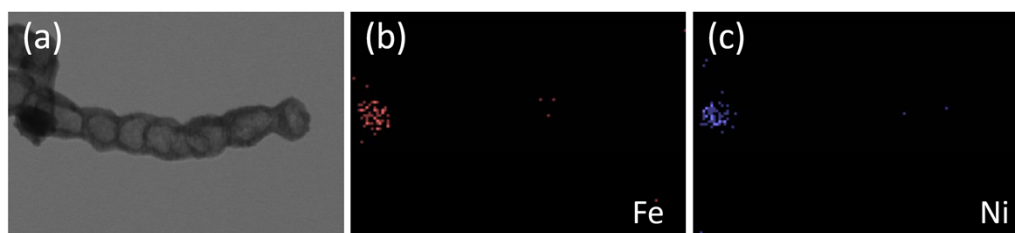


Fig. S6 (a) HAADF-STEM image of the CNTs on the side of the capsule, and the corresponding HAADF-STEM-EDS mapping of (b) Fe and (c) Ni elements, respectively.

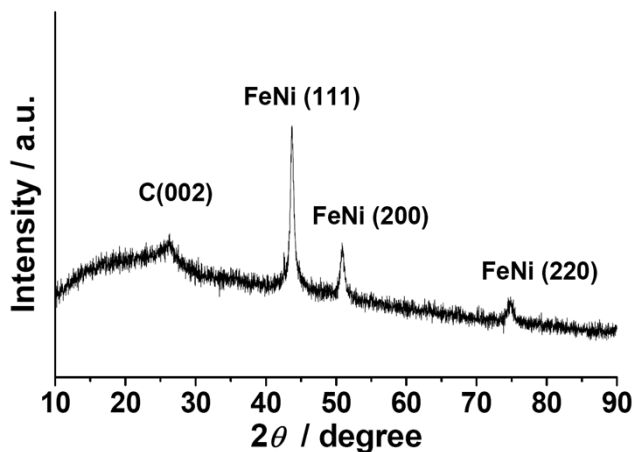


Fig. S7 XRD pattern of N-CC@CNTs before treated with HCl solution. The peaks at $2\theta \approx \text{ca. } 44^\circ, 51^\circ$ and 75° correspond to the (111), (200) and (220) planes of face-centered cubic (fcc) structure of FeNi alloy (JCPDS ICDD card NO. 47-1405).

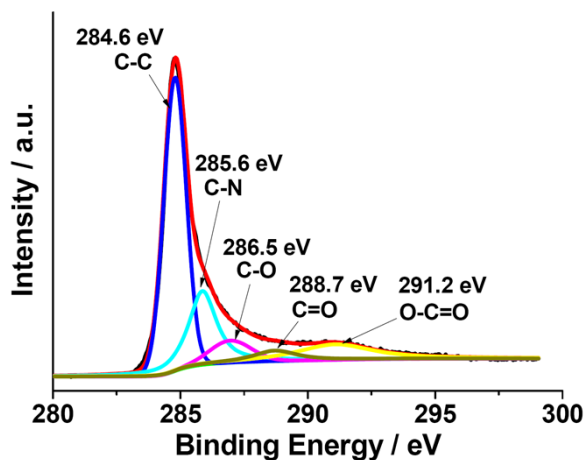


Fig. S8 High-resolution XPS spectrum of C1s peak for N-CC@CNTs.

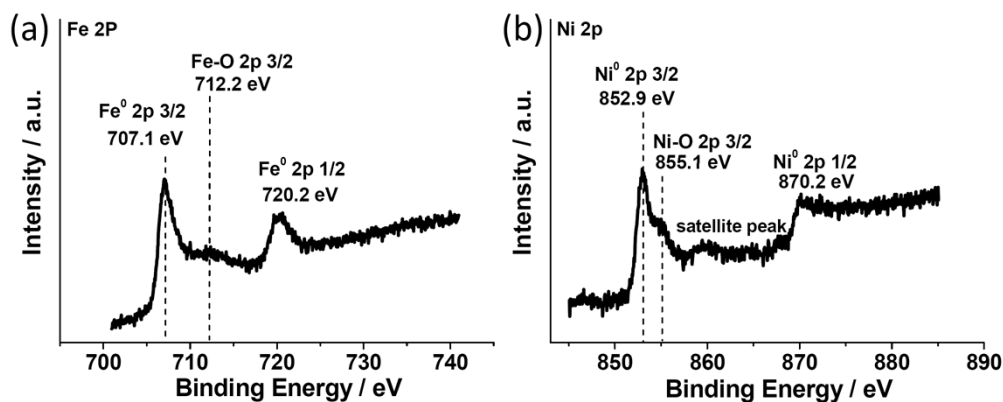


Fig. S9 The high-resolution XPS spectra of Fe 2p (a) and Ni 2p (b) peaks in N-CC@CNTs.

Fig. S9 presents the XPS spectra of Fe 2p and Ni 2p peaks in N-CC@CNTs. The main peaks at ca. 707.1 eV in (Fig. S8a) is very close to the reported 706.8 eV of Fe 2p_{3/2} for metallic Fe,^{s1} indicating that most the Fe species in the alloy particles was in its metallic form; and the main peak of Ni species in Fig. S8b located at 852.9 eV, attributing to the Ni 2p_{3/2} of metallic Ni (852.7 eV).^{s2} The results illustrated the alloy forms of Fe and Ni elements. The coexistence of “M-O” binds on the sample, suggesting the formation of M-O_{ads} or the surfaces of the Fe/Ni elements were partially oxidized to MO_x. The results are consistent with other observations of metallic metals at nanoscale.^{s3}

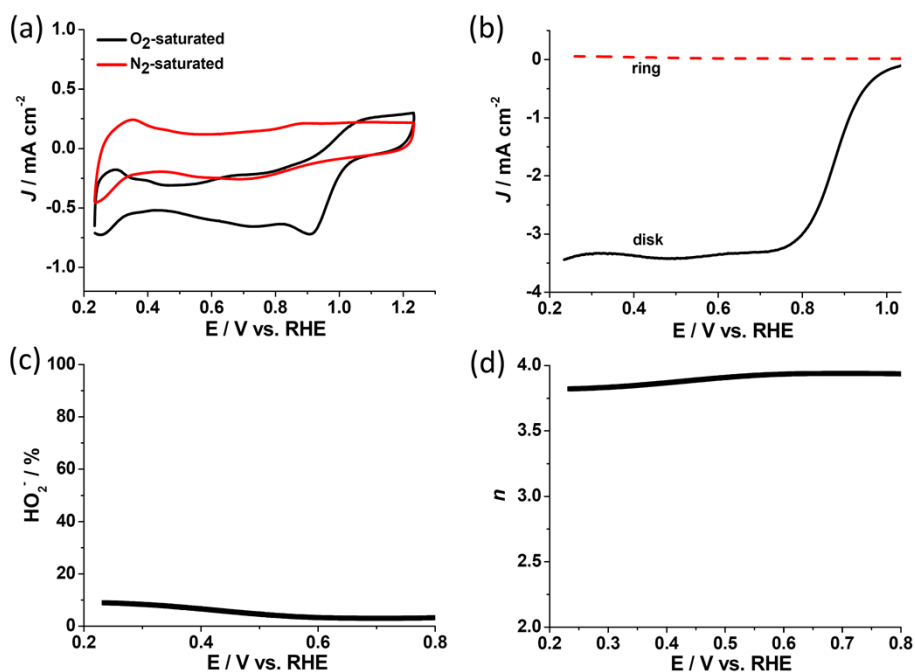


Fig. S10 (a) CVs of 20% Pt/C catalyst in O₂-saturated 0.1M KOH solution at a scan rate of 10 mV s⁻¹. (b) RRDE voltammograms for oxygen reduction in O₂-saturated 0.1 M KOH for the 20% Pt/C catalyst at 1500 rpm and 10 mV s⁻¹. (c) The peroxide percentage (%HO₂⁻) according to LSVs obtained for 20% Pt/C catalyst. (d) n obtained for 20% Pt/C catalyst according to LSV at 1500 rpm.

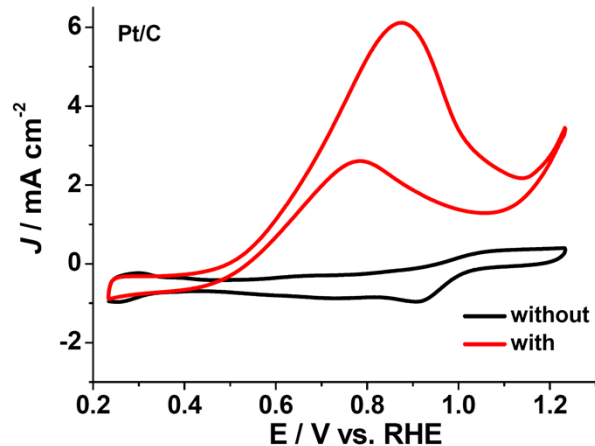


Fig. S11 CVs of 20% Pt/C catalyst in O_2 -saturated 0.1 M KOH with and without 10 vol% methanol at a scan rate of 10 mV s^{-1} .

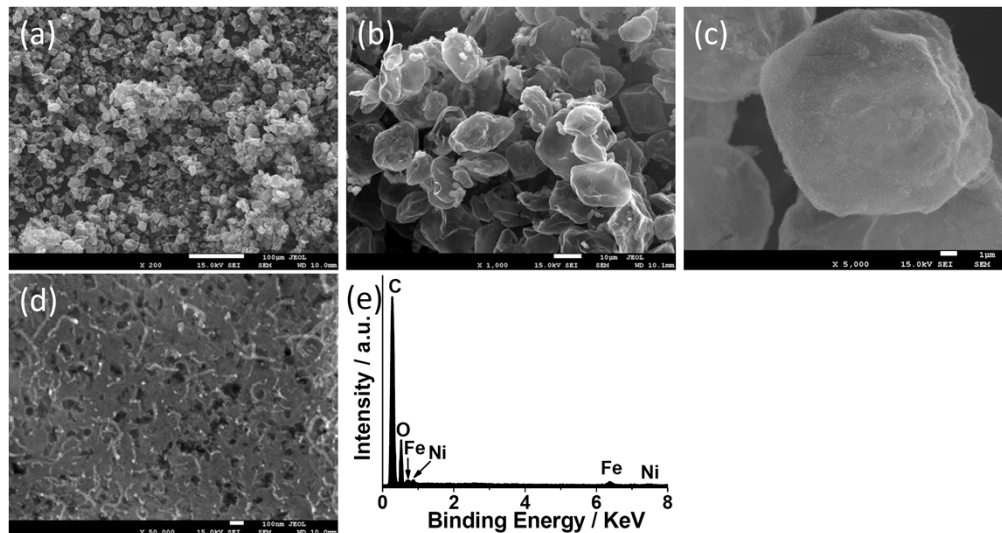


Fig. S12 (a–d) SEM images of N-CC@CNTs (1) at different magnifications. (e) The corresponding EDS spectroscopy. Scale bars: (a), 100 μm ; (b), 10 μm ; (c), 1 μm ; (d), 100 nm.

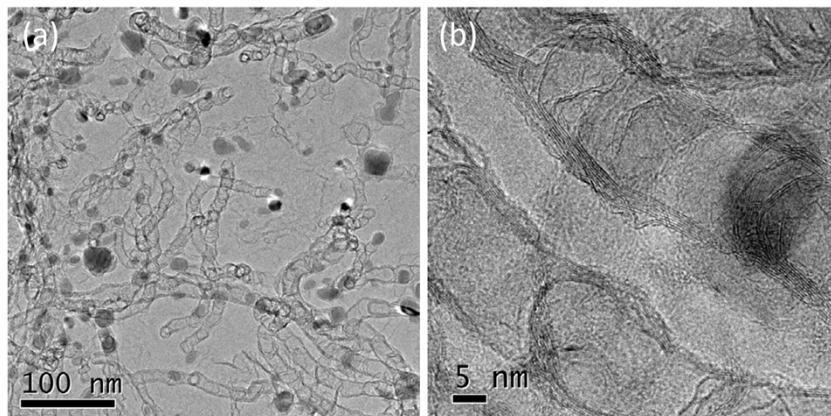


Fig. S13 (a, b) TEM images of the N-CC@CNTs (1) at different magnifications.

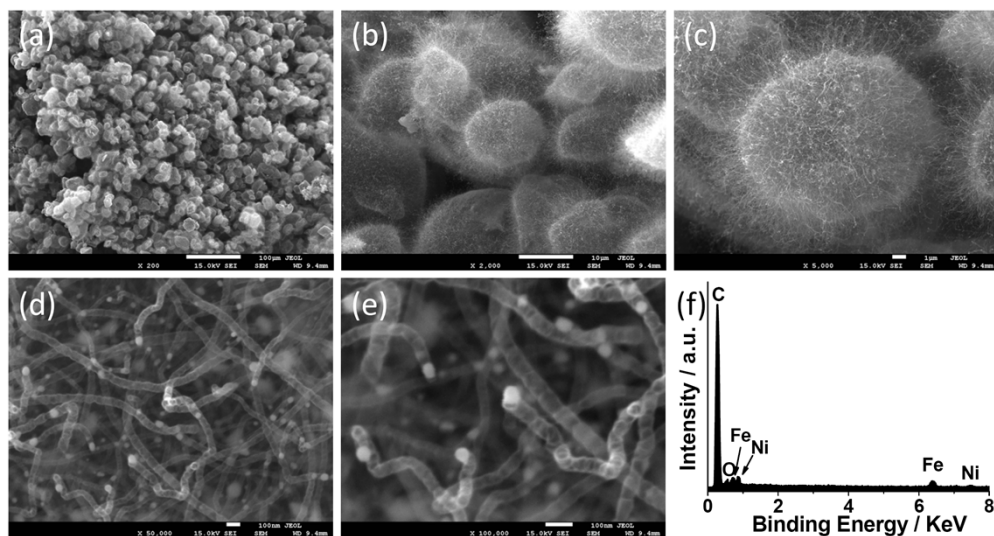


Fig. S14 (a–e) The SEM images of N-CC@CNTs (3) at different magnifications. (f) The corresponding EDS spectroscopy. Scale bars: (a), 100 μm ; (b), 10 μm ; (c, d), 1 μm ; (e), 100 nm.

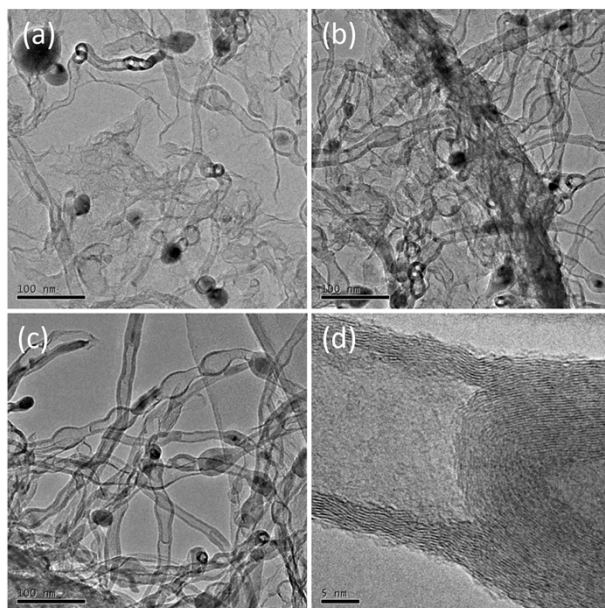


Fig. S15 TEM images of the N-CC@CNTs (3) at different magnifications.

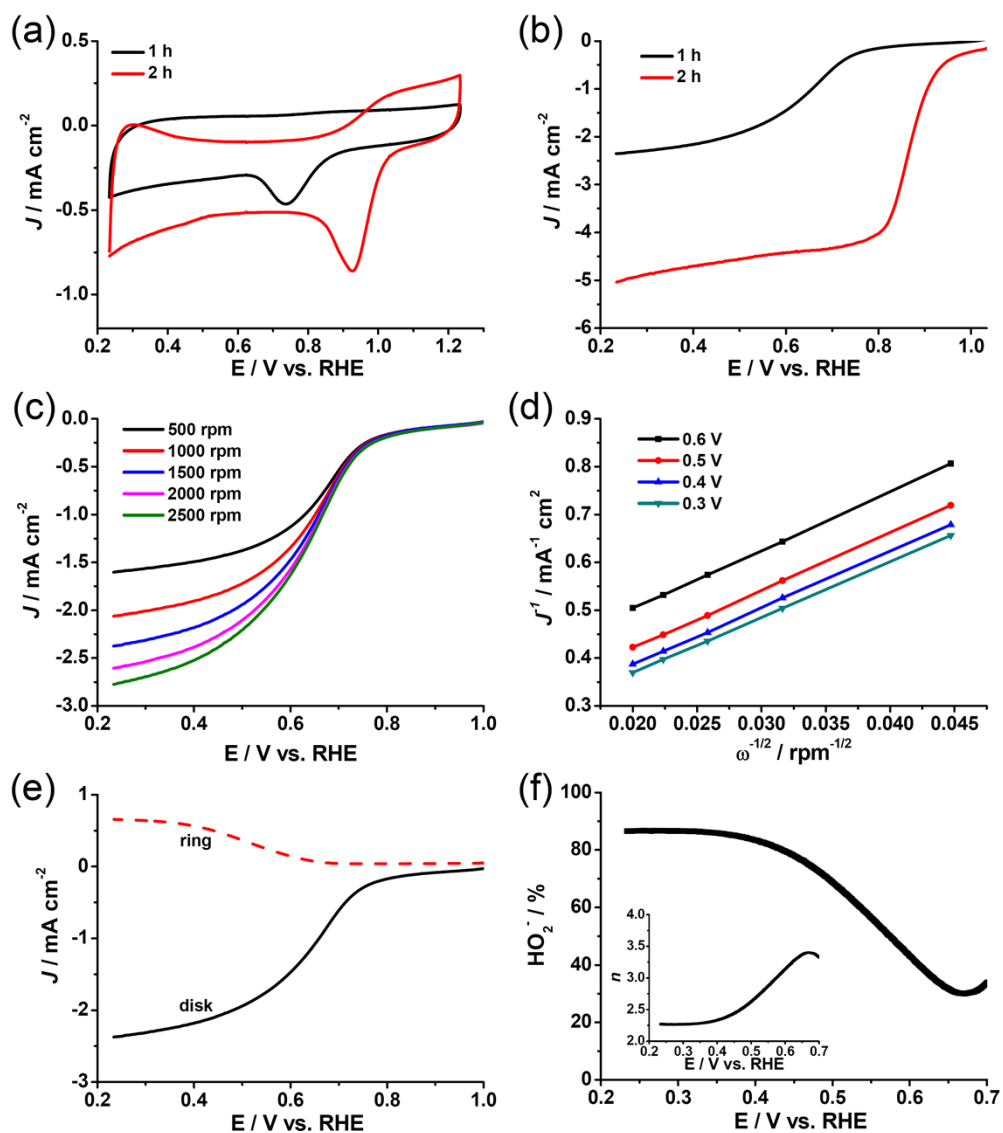


Fig. S16 (a) CVs of N-CC@CNTs and N-CC@CNTs (1) in O₂-saturated 0.1M KOH solution at a scan rate of 10 mV s⁻¹. (b) LSVs of N-CC@CNTs and N-CC@CNTs (1) with a RDE at 1500 rpm and scan rate of 10 mV s⁻¹. (c) LSVs obtained for N-CC@CNTs (1) at various speeds. (d) Koutecky–Levich plots for N-CC@CNTs (1) obtained from LSVs in (c) at different potentials. (e) RRDE voltammograms for oxygen reduction in O₂-saturated 0.1 M KOH for the N-CC@CNTs (1) electrode at 1500 rpm and 10 mV s⁻¹. (f) The peroxide percentage (%HO₂⁻) of N-CC@CNTs (1) as a function of the electrode potential obtained at 1500 rpm. The insert in (f) reflects the dependence of *n* of N-CC@CNTs (1) on the potential. Noticeably, N-CC@CNTs (1) showed a simultaneously increasing current density along with overpotential at all rotation speeds (Fig. S16c), indicating a surface dominant reaction without diffusion limited current, which is possibly due to the difficulties in reactant transfer with limited pores.

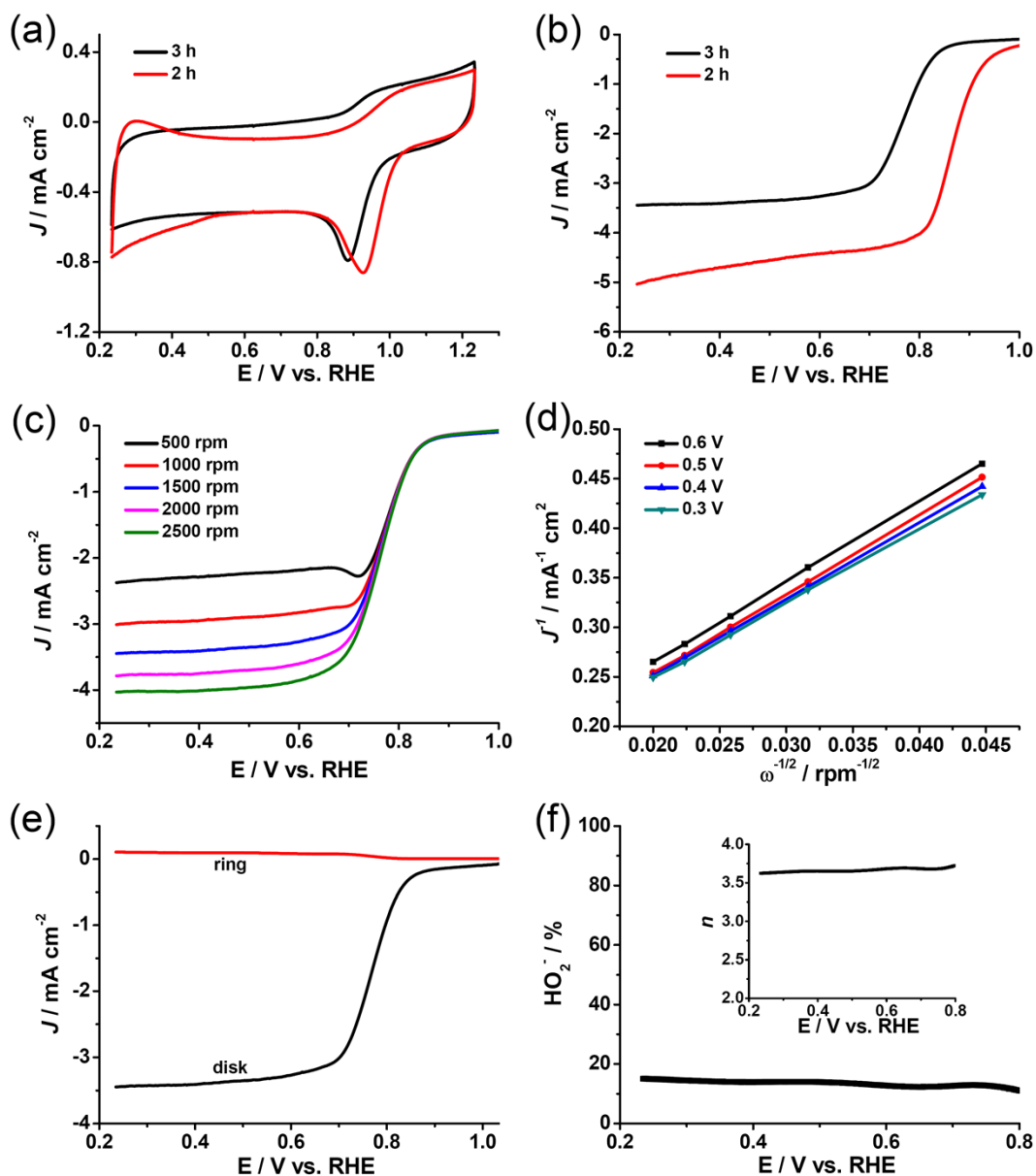


Fig. S17 (a) CVs of N-CC@CNTs and N-CC@CNTs (3) in O₂-saturated 0.1M KOH solution at a scan rate of 10 mV s⁻¹. (b) LSVs of N-CC@CNTs and N-CC@CNTs (3) with a RDE at 1500 rpm and scan rate of 10 mV s⁻¹. (c) LSVs obtained for N-CC@CNTs (3) at various speeds. (d) Koutecky–Levich plots for N-CC@CNTs (3) obtained from LSVs in (c) at different potentials. (e) RRDE voltammograms for oxygen reduction in O₂-saturated 0.1 M KOH for the N-CC@CNTs (3) electrode at 1500 rpm and 10 mV s⁻¹. (f) The peroxide percentage (%HO₂⁻) of N-CC@CNTs (3) as a function of the electrode potential obtained at 1500 rpm. The insert in (f) reflects the dependence of *n* of N-CC@CNTs (3) on the potential.

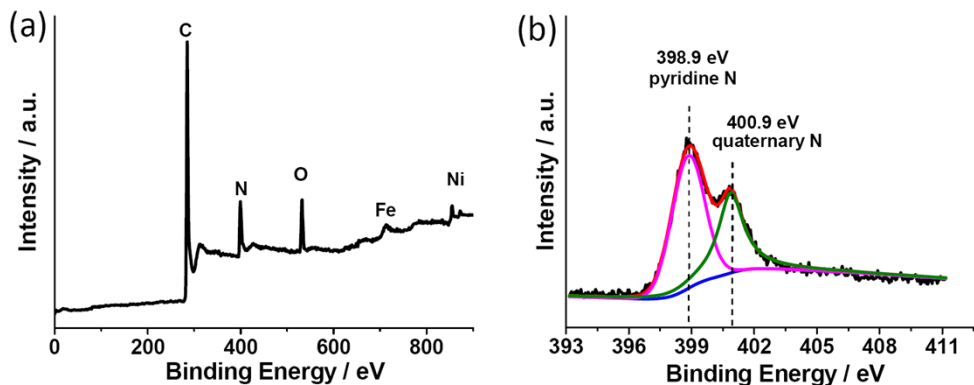


Fig. S18 (a) XPS spectrum of the N-CC@CNTs (1). (b) The high-resolution spectrum of N1s peak in (a).

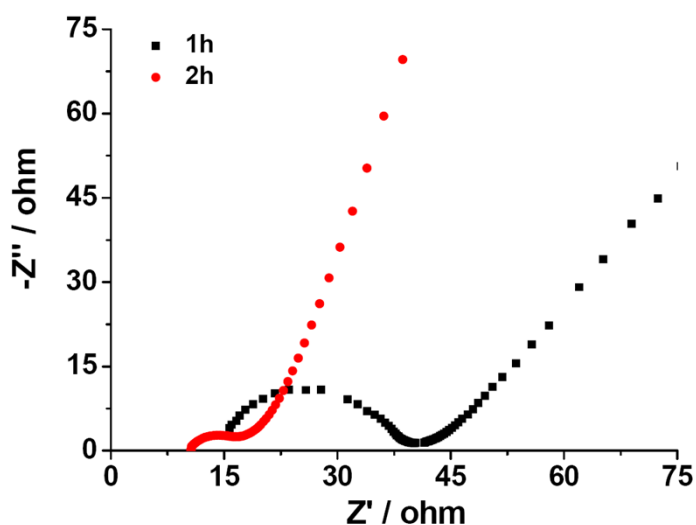


Fig. S19 Electrochemical impedance spectroscopy (EIS) of the N-CC@CNTs and N-CC@CNTs (1).

The EIS reported here were measured in a three-electrode cell by using a CHI760D electrochemical workstation. Impedance spectra were obtained at frequencies between 10 KHz and 0.01 Hz. The integration time was set at 10 s. EIS can give information about the comparison of the value on the resistances of N-CC@CNTs pyrolysed for 1 h and 2 h based on the impedance changes. Fig. S19 illustrates the results of impedance spectroscopy on the two electrodes in presence of 0.1 M O_2 saturated KOH solution (electrolyte for ORR test). The electrode of N-CC@CNTs (1) had an obvious increased semicircle when compared with N-CC@CNTs, implying high resistance of the sample,

resulting from the incomplete carbonization. However, after N-CC@CNTs were modified onto the electrode, the resistance decreased gradually, which attributed to N-CC@CNTs pyrolysed for 2 h had reduced interface thermal and electrical resistances, and thus promoted electron transfer.

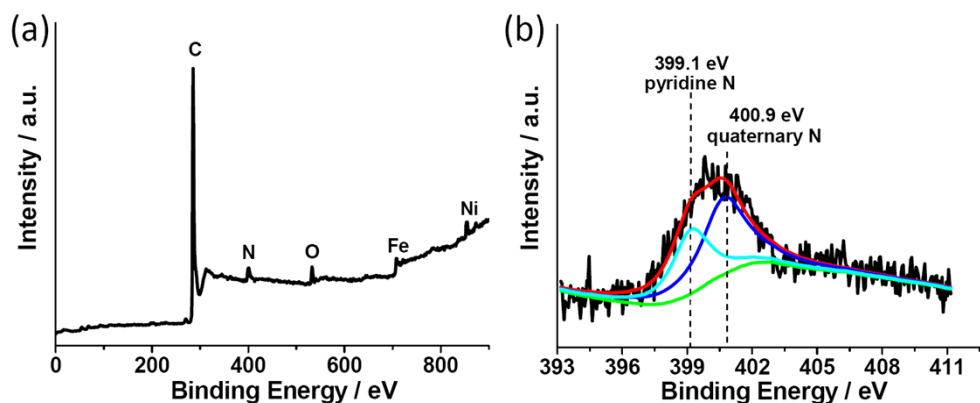


Fig. S20 (a) XPS survey spectrum of the N-CC@CNTs (3). (b) The high-resolution spectra of N 1s peak in (a).

Additionally, N-CC@CNTs treated at 800 °C for 1h (Fig. S12, S13) and 3h (Fig. S14, S15) were obtained for comparison, and labeled as N-CC@CNTs (1) and N-CC@CNTs (3), respectively. They were also tested under the same conditions for ORR. Those samples exhibit more negative onset potentials, lower cathodic density, higher H₂O₂ yield, and smaller *n* when compared with typical N-CC@CNTs (Fig. S16 and S17, Table S3), indicating the more negligible ORR catalytic activity. It is worth mentioning that the N-CC@CNTs (1) possess the highest content of N element (Fig. S18) among all of the samples, however, of which the ORR catalytic activity is lowest. This phenomenon can be explained by the conductivity of N-CC@CNTs (1) through a short time of thermal treatment is poor (Fig. S19). The N-CC@CNTs (3) displayed the extremely low N content of 1.8% (Fig. S20), resulting in relatively low activity towards ORR. That is, apart from the structure factor, both the conductivity and N content within the samples should be balanced.

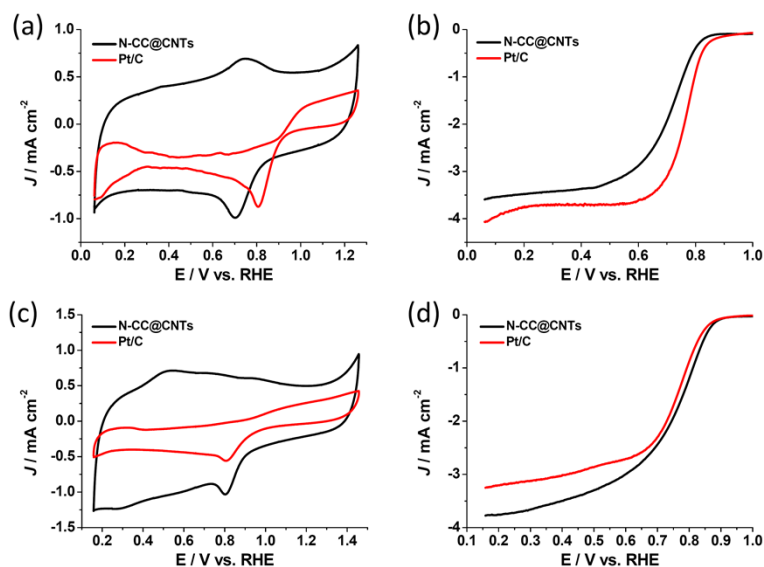


Fig. S21 Catalytic activity towards electrochemical reduction of oxygen in acidic and neutral solutions. (a, c) CVs of N-CC@CNTs and Pt/C in 0.1 M O₂-saturated HClO₄ aqueous solution and 0.1 M neutral phosphate buffer solution (PBS), respectively. The scan rate is 10 mV s⁻¹. (b, d) LSVs of N-CC@CNTs and Pt/C with a RDE at 1500 rpm and scan rate of 10 mV s⁻¹ in 0.1 M O₂-saturated HClO₄ aqueous solution and 0.1 M PBS, respectively.

Fig. S21 shows the ORR performance of the N-CC@CNT conditions are carried out in 0.1 M HClO₄ aqueous solution and 0.1 M PBS; and the corresponding results are added in the revised manuscript.

In a solution of 0.1 M O₂-saturated HClO₄ solution, a characteristic oxygen reduction peak appeared on the CV curve and the E_{1/2} for N-CC@CNTs estimated from the RDE plots were ca. 0.81 V vs. RHE (+0.55 V vs. Ag/AgCl), and ca. 0.71 V vs. RHE (+0.45 V vs. Ag/AgCl), respectively. These values of N-CC@CNTs are more negative than those of commercial Pt/C, indicating the activity of N-CC@CNTs towards ORR in acidic solutions was not as well as that in alkaline media. However, when the ORR occurred in neutral solution of PBS (pH=7), the oxygen reduction peak and the E_{1/2} for N-CC@CNTs were located at ca. 0.81 V vs. RHE (+0.15 V vs. Ag/AgCl), and ca. 0.80 V vs. RHE (+0.14 V vs. Ag/AgCl), respectively. The corresponding value of E_{1/2} for N-CC@CNTs with the comparable oxygen reduction peak value and a ca. 0.3 V E_{1/2} than that of Pt/C (+0.77 V vs. RHE, and +0.11 V vs. Ag/AgCl); also the limiting current density of N-CC@CNTs is substantially higher than that of Pt/C, showing the superior performance N-CC@CNTs owned to state-of-the-art Pt/C catalyst.

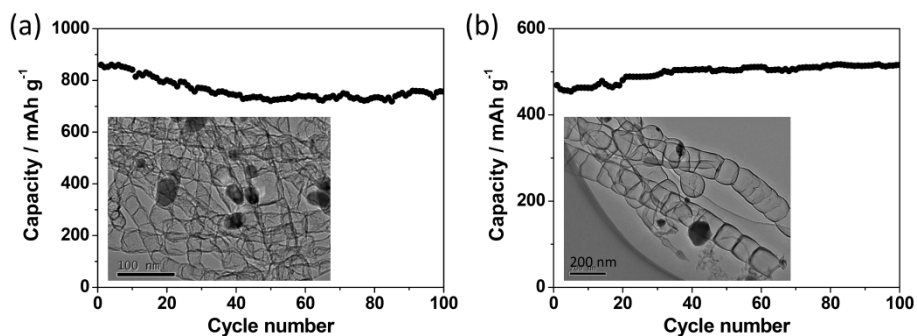


Fig. S22 Capacity vs. cycle number and the corresponding Columbic efficiency of the (a) N-CC@CNTs (Fe) and (b) N-CC@CNTs (Ni) at the current density of 500 mA g^{-1} for 100 cycles after being activated for five cycles at a current density of 100 mA g^{-1} . The insert in (a) and (b) are the TEM images of bamboo-like CNTs derived from Fe and Ni catalysts.

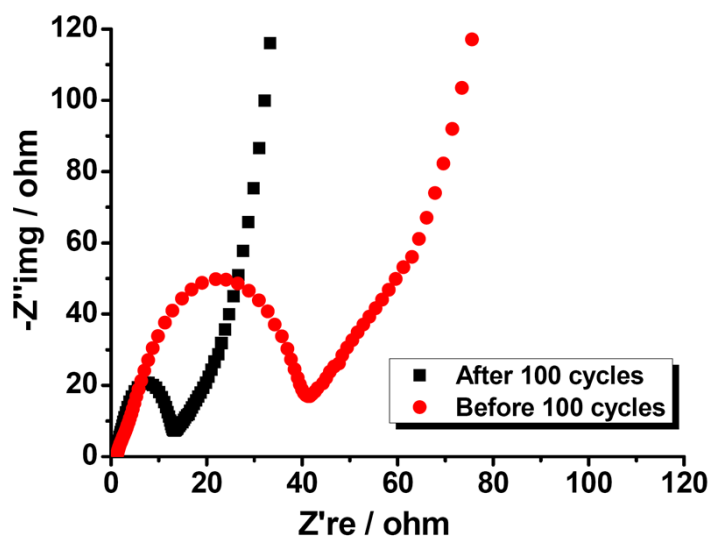


Fig. S23 Electrochemical impedance spectroscopy of the N-CC@CNTs before and after 50 cycles at the current density of 100 mA g^{-1} .

Table S1. Comparison of ORR electrocatalytic performance of N-CC@CNTs with some carbon-based ORR catalysts in alkaline solution reported previously.

Samples	Loading (mg cm^{-2})	Half-wave potential (V) ($E_{1/2}$ vs RHE)	TEN (N)	Electro lyte	Activity vs. Pt/C	Ref.

N-CC@CNTs	0.09	0.88	3.83~3.94	0.1M KOH	better	This work
CNT-G	0.485	~0.87	unknown	0.1M KOH	comparable	S4
N-CNT Arrays	unknown	~0.8	1.8~3.9	0.1M KOH	comparable	S5
N-doped G	unknown	~0.6	3.6-4.0	0.1M KOH	worse	S6
g-C ₃ N ₄ /carbon composite	~0.085	~0.70	3.12	0.1M KOH	worse	S7
N-graphene	0.051	~0.73	~3.91	0.1M KOH	worse	S8
N-doped carbon	~0.026	~0.69	~3.89	0.1M KOH	worse	S9
N-doped carbon nanocages	0.025	~0.74	3.27	0.1M KOH	worse	S10
S-Doped G	unknown	~0.73	~3.82	0.1M KOH	worse	S11
P-doped carbon	0.790	~0.72	~3.91	0.1M KOH	worse	S12
P-doped G	0.051	~0.71	3.0~3.8	0.1M KOH	worse	S13
I-doped G	0.076	~0.72	~3.9	0.1M KOH	worse	S14
N,F-codoped carbon	0.39	~0.87	~4	0.1M KOH	better	S15
B,N-doped CNTs	unknown	~0.75	~3.7	0.1M KOH	worse	S16
N,S-codoped G	unknown	~0.70	3.3~3.6	0.1M KOH	worse	S17

N,S-codoped carbon	0.28	~0.82	~3.77	0.1M KOH	worse	S18
Fe,N,S-codoped carbon	0.1	~0.81	3.6~4.0	0.1M KOH	worse	S19
N-doped G supported Fe ₃ O ₄	0.01	0.59	3.71-3.95	0.1M KOH	worse	S20
Co ₃ O ₄ /N-G	0.1	~0.83	3.9	0.1M KOH	worse	S21
Mn ₃ O ₄ /rGO	~0.085	~0.70	3.5	0.1M KOH	worse	S22
Fe/Terpyridine-GO	unknown	~0.68	3.6~3.9	0.1M KOH	worse	S23
N-Fe-CNT/CNP composite	0.2 1.0	0.87 0.93	3.92~4	0.1M NaOH	worse better	S24
Fe/Fe ₃ C-Melamine	0.286	~0.76	3.7~3.85	0.1M KOH	worse	S25
Co-/Fe-pyrolyzed polymer	0.5	0.76	3.96	PBS	worse	S26
Co ₃ O ₄ /G	0.708	~0.62	~4	0.1M KOH	worse	S27
MnCo ₂ O ₄ /N-doped G	0.100	~0.86	~3.9	0.1M KOH	worse	S28
nanocrystalline spinels	unknown	~0.73V	~3.7	0.1M KOH	worse	S29

Note: All the potentials were referred to RHE.^{S30,S31} GO and G stand for graphene oxide and reduced graphene oxide (also graphene), respectively.

Table S2. Comparison of the capacity for different carbon-based samples as anodes.

Sample	Current density (A g ⁻¹)	Capacity (mAh g ⁻¹)	Ref.
N-CC@CNTs	0.1	1450	This work
	0.5	1373	
	5	947	
	20	604	
	45	481	
Carbon nanorings	0.4	1237	S32
Mesoporous G nanosheets	0.1	770	S33
	0.5	430	
	2	280	
	5	225	
Mesoporous Carbon-CNTs	0.1	786	S34
	1.86	215	
CNTs/Carbon Nanofiber	0.1	1150	S35
	0.5	940	
	8	320	
CNTs/carbon nanospheres	0.05	965	S36
	3.7	330	
Graphene-based mesoporous carbon	0.07	770	S37
	0.37	540	
	1.86	370	
N-rich mesoporous carbons	0.1	825	S38

N-Doped Carbon Nanofibers	0.1	1280	S39
	2	637	
	5	505	
	20	226	
Mesoporous N-rich carbons	0.1	1365	S40
	0.5	700	
N-doped G	0.05	872	S41
	5	296	
	25	199	
B-doped G	0.05	1227	
	5	380	
	25	235	
N,S-co-doped porous G	0.1	957	S42
	0.5	860	
	2	700	
	5	560	
	20	380	
Fe ₂ O ₃ / G networks	0.2	864	S43
	0.5	854	
	2	718	
	5	587	
Mn ₃ O ₄ /G	0.4	730	S44
	1.6	390	
SnO ₂ @carbon	1	700	S45
SnO ₂ /G	0.1	878	S46
	2	519	
TiO ₂ nanocrystals/G sheets	0.1	189	S47

Fe ₃ O ₄ /G	0.093	744	S48
Fe ₃ O ₄ -CNT nanocomposite	0.09	919	S49
V ₃ O ₇ @graphene scrolls	2	138	S50
MnO/C	0.1	755.6	S51
G	0.05	<900	S52
G/Co ₃ O ₄	0.05	753	
ZnCo ₂ O ₄ @carbon nanofibers	0.2	560	S53
SnO ₂ @N-G	0.5	1074	S54
	2	915	
	5	782	
	20	417	
G-Nanotube-Iron	0.1	1024	S55
Ferrite/Carbon Hybrid	0.1	600	S56
	5	490	
G/Sn/G	0.05	590	S57
Ge@C/G	0.05	894	S58
	3.6	380	
Nano-Sn/C	0.2	710	S59
Sn/N-C	0.2	740	S60
	0.5	700	
	2	560	
	5	480	

CNTs/Cu _x O _y /Cu	0.5	474	S61
	1.86	418	
	18.6	220	
C@FeS	0.1	615	S62
MoS _x /CNTs	0.05	1126	S63

Table S3. The comparison of the electrochemical catalytic properties toward ORR of different samples.

Samples	Onset potential (V) Speed :1500 rmp	Disk current (mA) at -0.4 V	The yield of H ₂ O ₂ (%) (from -0.2/-0.3 V to -0.8 V)	ETN (n)?? (from -0.2/-0.3 V to -0.8 V)
N-CC@CNTs	-0.04	-3.5	3.1% ~ 8.8%	3.83 ~ 3.94
ETEK-20% catalyst	Ca. 0	-3.4	3.0% ~ 8.8%	3.82 ~ 3.94
N-CC@CNTs (1)	-0.24	-1.2	29.9% ~ 86.6%	2.27 ~ 3.40
N-CC@CNTs (3)	-0.13	-3.2	9.8% ~ 15.1%	3.63 ~ 3.75

References

- s1. D. H. Deng, L. Yu, X. Q. Chen, G. X. Wang, L. Jin, X. L. Pan, J. Deng, G. Q. Sun and X. H. Bao, *Angew. Chem. Int. Ed.*, 2013, **52**, 371.
- s2. I. Mintsouli, J. Georgieva, E. Valova, S. Armyanov, A. Kakaroglou, A. Hubin, O. Steenhaut, J. Dille, A. Papaderakis, G. Kokkinidis and S. Sotiropoulos, *J. Solid State Electrochem.*, 2013, **17**, 435.
- s3. C. G. Hu, Y. X. Cao, L. Yang, Z. Y. Bai, Y. M. Guo, K. Wang, P. L. Xu and J. G. Zhou, *Appl. Surf. Sci.*, 2011, **257**, 7968.

- S4. Y. G. Li, W. Zhou, H. L. Wang, L. M. Xie, Y. Y. Liang, F. Wei, J. C. Idrobo, S. J. Pennycook and H. J. Dai, *Nat. Nano.*, 2012, **7**, 394.
- S5. K. P. Gong, F. Du, Z. H. Xia, M. Durstock and L. M. Dai, *Science*, 2009, **323**, 760.
- S6. L. T. Qu, Y. Liu, J. B. Baek and L. M. Dai, *ACS Nano*, 2010, **4**, 1321.
- S7. J. Liang, Y. Zheng, J. Chen, J. Liu, D. Hulicova-Jurcakova, M. Jaroniec and S. Z. Qiao, *Angew. Chem. Int. Ed.*, 2012, **51**, 3892.
- S8. K. Parvez, S. Yang, Y. Hernandez, A. Winter, A. Turchanin, X. Feng and K. Müllen, *ACS Nano*, 2012, **6**, 9541.
- S9. R. L. Liu, D. Q. Wu, X. L. Feng and K. Müllen, *Angew. Chem. Int. Ed.*, 2010, **49**, 2565.
- S10. S. Chen, J. Y. Bi, Y. Zhao, L. J. Yang, C. Zhang, Y. W. Ma, Q. Wu, X. Z. Wang and Z. Hu, *Adv. Mater.*, 2012, **24**, 5593.
- S11. Z. Yang, Z. Yao, G. F. Li, G. Y. Fang, H. G. Nie, Z. Liu, X. M. Zhou, X. A. Chen and S. M. Huang, *ACS Nano*, 2011, **6**, 205.
- S12. D. S. Yang, D. Bhattacharjya, S. Inamdar, J. Park and J. S. Yu, *J. Am. Chem. Soc.*, 2012, **134**, 16127.
- S13. C. Z. Zhang, N. Mahmood, H. Yin, F. Liu and Y. L. Hou, *Adv. Mater.*, 2013, **25**, 4932.
- S14. I. Y. Jeon, H. J. Choi, M. Choi, J. M. Seo, S. M. Jung, M. J. Kim, S. Zhang, L. P. Zhang, Z. H. Xia, L. M. Dai, N. Park and J. B. Baek, *Sci. Rep.*, 2013, **3**, 1810.
- S15. X. J. Sun, P. Song, Y. W. Zhang, C. P. Liu, W. L. Xu and W. Xing, *Sci. Rep.*, 2013, **3**, 2505.
- S16. S. Y. Wang, E. Iyyamperumal, A. Roy, Y. H. Xue, D. S. Yu and L. M. Dai, *Angew. Chem.*, 2011, **123**, 11960.
- S17. J. Liang, Y. Jiao, M. Jaroniec and S. Z. Qiao, *Angew. Chem. Int. Ed.*, 2012, **51**, 11496.
- S18. X. F. Liu and M. Antonietti, *Adv. Mater.*, 2013, **25**, 6284.
- S19. Y. Q. Chang, F. Hong, C. X. He, Q. L. Zhang and J. H. Liu, *Adv. Mater.*, 2013, **25**, 1794.
- S20. Z. S. Wu, S. Yang, Y. Sun, K. Parvez, X. Feng and K. Müllen, *J. Am. Chem. Soc.*, 2012, **134**, 9082.

- S21. Y. Y. Liang, Y. G. Li, H. L. Wang, J. G. Zhou, J. Wang, T. Regier and H. J. Dai, *Nat. Mater.*, 2011, **10**, 780.
- S22. J. S. Lee, T. Lee, H. K. Song, J. Cho and B. S. Kim, *Energy Environ. Sci.*, 2011, **4**, 4148.
- S23. S. G. Song, Y. H. Xue, L. F. Feng, H. Elbatal, P. S. Wang, C. N. Moorefield, G. R. Newkome and L. M. Dai, *Angew. Chem. Int. Ed.*, 2013, **53**, 1415.
- S24. H. T. Chung, J. H. Won and P. Zelenay, *Nat. Comm.*, 2013, **4**, 1922.
- S25. J. S. Lee, G. S. Park, S. T. Kim, M. Liu and J. Cho, *Angew. Chem. Int. Ed.*, 2013, **125**, 1026.
- S26. Y. Zhao, K. Watanabe and K. Hashimoto, *J. Am. Chem. Soc.*, 2012, **134**, 19528.
- S27. J. W. Xiao, Q. Kuang, S. H. Yang, F. Xiao, S. Wang and L. Guo, *Sci. Rep.*, 2013, **3**, 2300.
- S28. Y. Y. Liang, H. L. Wang, J. G. Zhou, Y. G. Li, J. Wang, T. Regier and H. J. Dai, *J. Am. Chem. Soc.*, 2012, **134**, 3517.
- S29. F. Y. Cheng, J. Shen, B. Peng, Y. D. Pan, Z. L. Tao and J. Chen, *Nat. Chem.*, 2011, **3**, 79.
- S30. Y. Gorlin and T. F. Jaramillo, *J. Am. Chem. Soc.*, 2010, **132**, 13612.
- S31. R. G. Cao, R. Thapa, H. Kim, X. D. Xu, M. G. Kim, Q. Li, N. Park, M. L. Liu and J. Cho, *Nat. Comm.*, 2013, **4**, 2076.
- S32. J. Sun, H. M. Liu, X. Chen, D. G. Evans, W. S. Yang and X. C. Duan, *Adv. Mater.*, 2013, **25**, 1125.
- S33. Y. Fang, Y. Y. Lv, R. C. Che, H. Y. Wu, X. H. Zhang, D. Gu, G. F. Zheng and D. Y. Zhao, *J. Am. Chem. Soc.*, 2013, **135**, 1524.
- S34. B. K. Guo, X. Q. Wang, P. F. Fulvio, M. F. Chi, S. M. Mahurin, X. G. Sun and S. Dai, *Adv. Mater.*, 2011, **23**, 4661.
- S35. Y. M. Chen, X. Y. Li, K. Park, J. Song, J. H. Hong, L. M. Zhou, Y. W. Mai, H. T. Huang and J. B. Goodenough, *J. Am. Chem. Soc.*, 2013, **135**, 16280.
- S36. Y. M. Chen, Z. G. Lu, L. M. Zhou, Y. W. Mai and H. T. Huang, *Energy Environ. Sci.*, 2012, **5**, 7898.
- S37. S. B. Yang, X. L. Feng, L. Wang, K. Tang, J. Maier and K. Müllen, *Angew. Chem. Int. Ed.*, 2010, **49**, 4795.

- S38. Y. Mao, H. Duan, B. Xu, L. Zhang, Y. S. Hu, C. C. Zhao, Z. X. Wang, L. Q. Chen and Y. S. Yang, *Energy Environ. Sci.*, 2012, **5**, 7950.
- S39. L. Qie, W. M. Chen, Z. H. Wang, Q. G. Shao, X. Li, L. X. Yuan, X. L. Hu, W. X. Zhang and Y. H. Huang, *Adv. Mater.*, 2012, **24**, 2047.
- S40. Z. Li, Z. W. Xu, X. H. Tan, H. L. Wang, C. M. B. Holt, T. Stephenson, B. C. Olsen and D. Mitlin, *Energy Environ. Sci.*, 2013, **6**, 871.
- S41. Z. S. Wu, W. C. Ren, L. Xu, F. Li and H. M. Cheng, *ACS Nano*, 2011, **5**, 5463.
- S42. Z. L. Wang, D. Xu, H. G. Wang, Z. Wu and X. B. Zhang, *ACS Nano*, 2013, **7**, 2422.
- S43. X. H. Cao, B. Zheng, X. H. Rui, W. H. Shi, Q. Y. Yan and H. Zhang, *Angew. Chem. Int. Ed.*, 2013, **125**, 1.
- S44. H. L. Wang, L. F. Cui, Y. Yang, H. S. Casalongue, J. T. Robinson, Y. Y. Liang, Y. Cui and H. J. Dai, *J. Am. Chem. Soc.*, 2010, **132**, 13978.
- S45. X. Huang, J. Chen, Z. Y. Lu, H. Yu, Q. Y. Yan and H. H. Hng, *Sci. Rep.*, 2013, **3**, 2317.
- S46. S. J. R. Prabakar, Y. H. Hwang, E. G. Bae, S. Shim, D. Kim, M. S. Lah, K. S. Sohn and M. Pyo, *Adv. Mater.*, 2013, **25**, 3307.
- S47. W. Li, F. Wang, S. S. Feng, J. X. Wang, Z. K. Sun, B. Li, Y. H. Li, J. P. Yang, A. A. Elzatahry, Y. Y. Xia and D. Y. Zhao, *J. Am. Chem. Soc.*, 2013, **135**, 18300.
- S48. W. Wei, S. B. Yang, H. X. Zhou, I. Lieberwirth, X. L. Feng and K. Müllen, *Adv. Mater.*, 2013, **25**, 2909.
- S49. Y. Wu, Y. Wei, J. P. Wang, K. L. Jiang and S. S. Fan, *Nano Lett.*, 2013, **13**, 818.
- S50. M. Y. Yan, F. C. Wang, C. H. Han, X. Y. Ma, X. Xu, Q. Y. An, L. Xu, C. J. Niu, Y. L. Zhao, X. C. Tian, P. Hu, H. G. Wu and L. Q. Mai, *J. Am. Chem. Soc.*, 2013, **135**, 18176.
- S51. Y. Xia, Z. Xiao, X. Dou, H. Huang, X. H. Lu, R. J. Yan, Y. P. Gan, W. J. Zhu, J. P. Tu, W. K. Zhang and X. Y. Tao, *ACS Nano*, 2013, **7**, 7083.
- S52. Z. S. Wu, W. C. Ren, L. Wen, L. B. Gao, J. P. Zhao, Z. P. Chen, G. G. Zhou, F. Li and H. M. Cheng, *ACS Nano*, 2010, **4**, 3187.
- S53. G. G. Zhang, B. Y. Xia, C. Xiao, L. Yu, X. Wang, Y. Xie and X. W. Lou, *Angew. Chem. Int. Ed.*, 2013, **52**, 8643.
- S54. X. S. Zhou, L. J. Wan and Y. G. Guo, *Adv. Mater.*, 2013, **25**, 2152.

- S55. S. H. Lee, V. Sridhar, J. H. Jung, K. Karthikeyan, Y. S. Lee, R. Mukherjee, N. Koratkar and I. K. Oh, *ACS Nano*, 2013, **7**, 4242.
- S56. B. Jang, M. Park, O. B. Chae, S. J. Park, Y. J. Kim, S. M. Oh, Y. Z. Piao and T. Hyeon, *J. Am. Chem. Soc.*, 2012, **134**, 15010.
- S57. B. Luo, B. Wang, X. L. Li, Y. Y. Jia, M. H. Liang and L. J. Zhi, *Adv. Mater.*, 2012, **24**, 3538.
- S58. D. J. Xue, S. Xin, Y. Yan, K. C. Jiang, Y. X. Yin, Y. G. Guo and L. J. Wan, *J. Am. Chem. Soc.*, 2012, **134**, 2512.
- S59. Y. H. Xu, Q. Liu, Y. J. Zhu, Y. H. Liu, A. Langrock, M. R. Zachariah and C. S. Wang, *Nano Lett.*, 2013, **13**, 470.
- S60. Z. Q. Zhu, S. W. Wang, J. Du, Q. Jin, T. R. Zhang, F. Y. Cheng and J. Chen, *Nano Lett.*, 2014, **14**, 153.
- S61. S. Venkatachalam, H. W. Zhu, C. Masarapu, K. H. Hung, Z. Liu, K. Suenaga and B. Q. Wei, *ACS Nano*, 2009, **3**, 2177.
- S62. C. Xu, Y. Zeng, X. H. Rui, N. Xiao, J. X. Zhu, W. Y. Zhang, J. Chen, W. L. Liu, H. T. Tan, H. H. Hng and Q. Y. Yan, *ACS Nano*, 2012, **6**, 4713.
- S63. Y. M. Shi, Y. Wang, J. I. Wong, A. Y. S. Tan, C. L. Hsu, L. J. Li, Y. C. Lu and H. Y. Yang, *Sci. Rep.*, 2013, **3**, 2169.